

Title	Oriented siloxane-containing vaterite/poly(lactic acid) composite scaffolds for controlling osteoblast alignment and proliferation
Author(s)	Lee, Sungho; Kiyokane, Yuriko; Kasuga, Toshihiro et al.
Citation	Journal of Asian Ceramic Societies. 2019, 7(2), p. 228-237
Version Type	VoR
URL	https://hdl.handle.net/11094/89824
rights	This article is licensed under a Creative Commons Attribution-NonCommercial 4.0 International License.
Note	

Osaka University Knowledge Archive : OUKA

<https://ir.library.osaka-u.ac.jp/>

Osaka University

Oriented siloxane-containing vaterite/poly(lactic acid) composite scaffolds for controlling osteoblast alignment and proliferation

Sungho Lee, Yuriko Kiyokane, Toshihiro Kasuga & Takayoshi Nakano

To cite this article: Sungho Lee, Yuriko Kiyokane, Toshihiro Kasuga & Takayoshi Nakano (2019) Oriented siloxane-containing vaterite/poly(lactic acid) composite scaffolds for controlling osteoblast alignment and proliferation, Journal of Asian Ceramic Societies, 7:2, 228-237, DOI: [10.1080/21870764.2019.1599528](https://doi.org/10.1080/21870764.2019.1599528)

To link to this article: <https://doi.org/10.1080/21870764.2019.1599528>



© 2019 The Author(s). Published by Informa UK Limited, trading as Taylor & Francis Group on behalf of The Korean Ceramic Society and The Ceramic Society of Japan



Published online: 04 Apr 2019.



Submit your article to this journal [↗](#)



Article views: 685



View related articles [↗](#)




View Crossmark data [↗](#)



Citing articles: 2 View citing articles [↗](#)

Oriented siloxane-containing vaterite/poly(lactic acid) composite scaffolds for controlling osteoblast alignment and proliferation

Sungho Lee ^a, Yuriko Kiyokane^a, Toshihiro Kasuga^b and Takayoshi Nakano^a

^aDivision of Materials and Manufacturing Science, Graduate School of Engineering, Osaka University, Osaka, Japan; ^bDivision of Advanced Ceramics, Graduate School of Engineering, Nagoya Institute of Technology, Nagoya, Japan

ABSTRACT

Bone tissue has an anisotropic structure, which is strongly associated with the collagen fibril orientation and the direction of the *c*-axis of the bone apatite crystal. The bone regeneration process contains two main phases: bone mineral density (BMD; bone quantity) restoration and reconstruction of the bone apatite *c*-axis orientation (bone quality), which is the dominant factor for the mechanical properties of bone. Hence, restoration of the bone quality and quantity is required for bone tissue regeneration. In this work, novel, oriented siloxane-containing vaterite/poly(lactic acid) composite scaffolds were developed by controlling the cell alignment and proliferation, which play an important role in regenerating the bone quality and quantity, respectively. Our strategy controlled the cell alignment and proliferation using a morphological design of the scaffolds and the ions released from the siloxane-containing vaterite. The scaffolds were designed to control of the cell alignment, which successfully induced cell orientation along the fibermats. In addition, the released ions from the siloxane-containing vaterite improved osteoblast proliferation, indicating that the released Mg²⁺ and silicate ions stimulated cell adhesion and proliferation. These results indicated that the fibermats developed in this work could be used for bone tissue regeneration scaffolds that enable the recovery of bone quality and quantity.

ARTICLE HISTORY

Received 5 February 2019
Accepted 18 March 2019

KEYWORDS

Biomaterial; bone anisotropy; bone quality; vaterite; electrospinning

1. Introduction

Bone is a highly calcified tissue consisting of collagen fibril and biological apatite (BAP) with several nanoscale to microscale hierarchical levels [1,2]. The multiscale structure of bone tissue indicates a highly anisotropic structure, which is strongly associated with the collagen fibril orientation and the direction of the *c*-axis of the BAP crystals [3,4]. The anisotropic microstructure of bone tissue is the most important bone quality index, dominating the mechanical properties of bone tissue rather than the bone mass (i.e. bone quantity) [5,6]. During the bone regeneration process, the reconstruction of the anisotropic bone microstructure is significantly delayed compared to the bone mineral density (BMD) restoration, which induces severe mechanical dysfunctions [5]. The development of biomaterials with a dual effect, such as a controllable bone quality and bone quantity, is required for the recovery of anisotropic healthy bone tissue.

Controlling the cell alignment is a valuable strategy for reconstructing anisotropic bone matrices [7,8]. Human mesenchymal stem cells (hMSCs) on poly(lactic acid) (PLLA) oriented nano-fibermats were highly aligned in the direction of the collector, where the cells were stretched along the long axis of the nano-fibers [9,10]. Subsequently, the collagen fibril bundles produced by the hMSCs were aligned in the direction

of the cell adhesion (i.e. nano-fiber direction). Chen *et al.* reported that oriented nanofibers upregulated the expression of osteogenic markers, such as the runt-related transcription factor (Runx-2), type I collagen, alkaline phosphatase (ALP), bone sialoprotein (BSP), and osteocalcin (OCN) [11]. In our previous study, the collagen/apatite matrix alignment was dependent on the osteoblast orientation [7,12]. Moreover, the osteoblast-produced collagen matrix was oriented in the direction of cellular elongation, and the *c*-axis of the BAP showed preferential alignment along the direction of the newly synthesized collagen fibers [7]. Accordingly, the directional control of the osteoblasts could affect the formation of anisotropic bone tissue (i.e. bone quality).

Vaterite (V) is the most thermodynamically unstable polymorph among the calcium carbonates, and it releases immediately Ca²⁺ and carbonate ions into the body fluid, which neutralizes the pH decrease at the inflamed implantation site. Siloxane-containing vaterite (SiV) particles were prepared as a carrier for silicate and Ca²⁺ ions, which can stimulate bone formation [13,14]. Recently, magnesium- and siloxane-containing vaterite particles were prepared, and the osteoblast proliferation, differentiation, and mineralization were enhanced by the dissolved silicate, Mg²⁺, and Ca²⁺ ions [15–17]. Xynos *et al.* reported that silicate and

Ca^{2+} ions stimulated human osteoblast proliferation by increasing the production of insulin-like growth factor II (IGF-II) [18] and up-regulating ALP and OCN, which are parameters of osteoblast differentiation [19]. The Ca^{2+} ion enhances osteoblast proliferation, differentiation, and extracellular matrix (ECM) mineralization [20,21]. The expression of various integrin family members, which are a class of adhesion proteins for the cells, was increased by the Mg^{2+} ion [22]. Moreover, the Mg^{2+} ion enhances osteoblast proliferation, differentiation, and mineralization [22–24]. Accordingly, controlling the therapeutic ion release from the biomaterials can enhance bone formation (i.e. bone quantity).

Electrospinning is a useful method to produce fibrous scaffolds, and the scaffolds can be applied to a biomimetic template for cell adhesion, proliferation, differentiation, and mineralization on damaged tissue. Obata *et al.* evaluated random SiV/PLLA fiber mats for a guided bone regeneration membrane [14]. When murine osteoblast-like cells (MC3T3-E1) were seeded, significantly larger numbers of cells were observed on the SiV/PLLA fiber mats than that of V/PLLA, which has no ability to release silicate ions. The expression of ALP was also significantly higher on the SiV/PLLA fiber mats. Hence, the released ions from SiV were expected to successfully enhance bone formation. *In vivo*, newly formed bone was observed in 4 weeks, and the defect was covered in 12 weeks. Kasuga *et al.* reported cotton-like SiV/PLLA composites prepared by an electrospinning method, and the composites showed excellent bioactivity and ease of handling for bone-filling surgery [25,26].

The aim of this work is to create a biomaterial for bone tissue regeneration, including the recovery of bone quality (i.e. BAp orientation). An anisotropic fibrous scaffold can control the alignment of cells. In our previous study, oriented bioactive glass/PLLA composite fiber mats were prepared for controlling osteoblast alignment by electrospinning [27]. The cell alignment was successfully controlled by the anisotropic morphology of the fiber mats. However, the cells on the fiber mats aligned $\pm 10^\circ$ to the fiber-orientated direction were approximately 46.5%, requiring further improvement. Sun *et al.* reported that the cells adhered on a single fiber when the diameter of the fiber was larger than 10 μm , whereas the cells adhered on several fibers with spreading when the diameter of the fibers was less than 10 μm [28]. Therefore, the alignment of the cells adhered on a single fiber could be easily controlled with the morphology of the fiber mats. Thus, the oriented fiber mats were prepared with a fiber diameter greater than 10 μm to control the cell alignment. SiV and MgSiV particles were used for the oriented fiber mats as a carrier of siloxane, Ca^{2+} , and Mg^{2+} ions, which were expected to stimulate bone formation (i.e. bone

quantity). PLLA, which is the most widely used biodegradable polymer in the biomaterial field, was chosen to fabricate the oriented fiber mat to control the cell alignment (i.e. bone quality). In this work, a fundamental investigation was performed to design orientated fiber mats for bone tissue regeneration with bone quality. SiV/PLLA- and MgSiV/PLLA-oriented fiber mats were prepared, and their morphology, ion-releasing ability, cell proliferation, and cell alignment on the fiber mats were evaluated.

2. Materials and methods

2.1. Preparation of the vaterites

V, SiV, and MgSiV particles were synthesized by a carbonation process with methanol following the method described in previous studies [15,29–31]. Briefly, the MgSiV particles were synthesized using the following process [15]. $\text{Mg}(\text{OH})_2$ (11.7 g, Wako Pure Chemical), $\text{Ca}(\text{OH})_2$ (133.4 g, Kishida Chemical Co.), and 3-aminopropyltriethoxysilane (60 mL, APTES, Dow Corning Co.) were mixed with methanol (2.0 L, Wako Pure Chemical) and distilled water (200 mL) while stirring at 21°C. Each reagent was added at 20-min intervals. Carbon dioxide gas was introduced to the slurry at a rate of 2.0 L min^{-1} for 60 min, resulting in a translucent precursor gel. The gel was aged for 12 h at room temperature (approximately 25°C) and then heated to 110°C for 24 h to remove the residual solvent. The SiV particles without $\text{Mg}(\text{OH})_2$ and the V particles as a control without $\text{Mg}(\text{OH})_2$ and APTES were prepared by a carbonation process. The particles were prepared by Yabashi Industries Co. The particles were observed using scanning electron microscopy (SEM, JSM-6500, JEOL) with an acceleration voltage of 15 kV after coating the samples with an amorphous osmium layer using an osmium coater (Neoc CS, Meiwa Fosis Co. Ltd.). The amount of Si and Mg in the SiV and MgSiV particles was estimated by an X-ray fluorescence analysis (RIX3000, Rigaku). The Si amounts of the SiV and MgSiV particles were 2.7 wt.% and 2.7 wt.%, respectively, and the Mg content of MgSiV was 2.0 wt.%. The density of the particles was measured by a pycnometer method using ethanol (99.5%, Nacal Tesque) as the immersion fluid.

2.2. Preparation of the composite pellets and oriented fiber mats

The V, SiV, and MgSiV particles were mixed with PLLA (LACEA, Mitsui Chemical) by a melt-blending method using a kneader (PBV-0.1, Irie Shokai) at 190°C for 10 min, resulting in composite pellets. The weight ratios of the V, SiV, and MgSiV particles in the composites were set to 60 wt.% and were denoted by VPC,

SiVPC, and MgSiVPC, respectively. The molecular weight distribution of the composites was determined by gel permeation chromatography (GPC, Prominence, Shimadzu) using a KF-806L column (Shodex). Detection was performed using a Shimadzu refractometer RID-10A. Chloroform (99.7%, HPLC grade, Wako Pure Chemical) was used as the eluent flowing at 1 mL min⁻¹ at 35°C. The composites were manually injected (20 µL) at concentrations ranging from 10 to 15 mg mL⁻¹. The average molecular weight and distribution were given against the linear polystyrene calibration.

The oriented fibermats were prepared by an electrospinning method. The composite pellets were dissolved in chloroform (99.0%, Wako Pure Chemical) at 6–14 wt.% of PLLA to prepare the solution for electrospinning. Subsequently, the prepared solutions were loaded into a syringe pump (FP-1100, Melquest, Japan) with a syringe needle (18 gauge), which was set at 2.5 µL·s⁻¹. A high-voltage supply (HARb-40P0.75, Matsusada Precision Inc.) was used to apply 16 kV to the needle tip. The distance between the needle tip and drum collector was maintained at 200 mm. The drum collector (φ 30 mm) was rotated at 3000 rpm (4.7 m·s⁻¹). The obtained fibermats were denoted as VPC_x, SiVPC_x, and MgSiVPC_x, where x ($x = 6–14$) is the wt.% of PLLA in the electrospinning solution. The electrospinning was carried out at room temperature (approximately 25°C) and approximately 40% relative humidity.

The morphology of the prepared fibermats was observed by SEM with an accelerating voltage of 3 kV after coating the samples with an amorphous osmium layer using an osmium coater. The fiber diameter and angle (θ) between the fiber and collector rotation direction were measured using ImageJ software (NIH).

2.3. Ion releasing behavior of the fibermats

To characterize the ion releasing behavior from VPC₇, SiVPC₈, and MgSiVPC₁₂, with a diameter of 14 mm and an approximate thickness of 150 µm, the fibermats were soaked in an alpha-minimum essential medium (α-MEM, with L-glutamine and phenol red, Invitrogen) containing 10% fetal bovine serum (FBS, Invitrogen) for 21 days (37°C, 5% CO₂). The samples were set in 24-well plates ($n = 9$) and immersed in 1 mL of α-MEM. Subsequently, the α-MEM was taken and replaced with 1 mL of fresh α-MEM at a preset time point. The concentrations of the Si, P, Ca²⁺, and Mg²⁺ ions in the α-MEM were measured by inductively coupled plasma atomic emission spectroscopy (ICP-AES, ICPS-8100, Shimadzu). The accumulative ion concentration is calculated as follows:

$$\sum(C_t - C_{MEM}), \quad (1)$$

where C_t is the concentration of the element in the α-MEM with VPC₇, SiVPC₈, and MgSiVPC₁₂ at time point t , and C_{MEM} is the element concentration in the α-MEM. A positive value represents the amount of ions released into the α-MEM, and a negative value indicates the amount of ions used for precipitation. The fibermats after soaking in the α-MEM for 21 days were analyzed by X-ray diffractometry (XRD, X'pert PRO, Phillips) using Cu Kα radiation.

2.4. Primary osteoblast isolation and culture on the fibermats

Primary osteoblasts were isolated from newborn mouse calvariae as described in our previous study [32]. In brief, calvariae from newborn C57BL/6 mice were excised under aseptic conditions and placed in an ice-cold α-MEM containing 10% FBS. Then, the fibrous tissues around the bone were gently removed. The calvariae were subjected to a series of collagenase (Wako Pure Chemical)/trypsin (Nacalai Tesque) digestions at 37°C for 15 min each. The first two digests were discarded because fibroblasts remained [33]. The supernatants of digests 3–5 were neutralized with α-MEM containing 10% FBS and were pooled. The pooled solutions were filtered using a 100-µm mesh. The filtrates were centrifuged, and the resulting pellets were resuspended in the α-MEM containing 10% FBS. VPC₇, SiVPC₈, and MgSiVPC₁₂ with a 14-mm diameter were prepared. The samples were soaked in 70% ethanol for 30 s and were subsequently dried under an ultraviolet (UV) light for 30 min for sterilization. The samples were placed into 24-well plates ($n = 3$), and the primary osteoblast cells were seeded by adding 1.0 mL of α-MEM containing the cells at a concentration of 5×10^4 cells·mL⁻¹. The culture medium was replaced after day 1 and day 3.

2.5. Fluorescence imaging of the primary osteoblasts

The primary osteoblasts were cultivated for 6 days on the samples ($n = 3$), and the cells were fixed with 4% formaldehyde in phosphate buffered saline (PBS) for 20 min. After washing three times with PBS-0.05% Triton X-100 (PBST), the cells were incubated with Alexa Fluor® 488-conjugated phalloidin (Invitrogen). Subsequently, the cells were washed and mounted in Fluoro-KEEPER antifade reagent with DAPI (Nacalai Tesque). Fluorescent images were obtained using a fluorescence microscope (BZ-8100, Keyence). The cell orientation angle (θ) against the collector rotation direction was analyzed using Cell Profiler software (Broad Institute Cambridge).

2.6. Quantitative analysis for the degrees of fiber and cell orientation

To evaluate the degrees of fiber and cell arrangement, the orientation order parameters FD and CD , respectively, was calculated [34]. This system was derived using a distribution function $n(\theta)$, which is defined as the number of measured fibers or cells at angle θ . The expected value of the mean square of cosine $\langle \cos^2\theta \rangle$, FD , and CD were calculated as follows.

$$\langle \cos^2\theta \rangle = \frac{\int_0^{2\pi} \cos^2\theta \cdot n(\theta) d\theta}{\int_0^{2\pi} n(\theta) d\theta} \quad (2)$$

$$FD \text{ or } CD = 2(\langle \cos^2\theta \rangle - 0.5) \quad (3)$$

The degrees of fiber and cell alignment FD and CD have a value ranging from -1 (fiber or cell completely aligned perpendicular to the collector rotation direction), 0 (fiber or cell oriented randomly), to 1 (fiber or cell completely aligned parallel to the collector rotation direction).

2.7. Osteoblasts proliferation on the fibermats

VPC_7 , $SiVPC_8$, and $MgSiVPC_{12}$ with an 8-mm diameter were prepared for an osteoblast proliferation test. The samples were soaked in 70% ethanol for 30 s and subsequently dried under a UV light for 30 min for sterilization. The cells were cultured in α -MEM containing 10% FBS. The samples were placed into 48-well plates ($n = 4$), and mouse osteoblast-like cells (MC3T3-E1 cells) were seeded by adding 0.5 mL of the α -MEM containing the cells at a concentration of 2×10^4 cells·mL⁻¹. The culture medium was replaced after 1 and 3 days of culture. After 1, 3, and 6 days of culture, the samples were washed with PBS, and 0.5 mL of α -MEM (no phenol red, Invitrogen) and 50 μ L of Cell Count Reagent SF (Nacalai Tesque) were added to the samples. After 2 h of incubation (37°C, 5% CO₂), the absorbance at 450 nm was evaluated using a microplate reader (Multiskan FC, Thermo Scientific). The number of cells was calculated

by a standard curve between the number of cells and the absorbance of the resulting medium.

2.8. Statistical analysis

Statistical significance was assessed by a one-way ANOVA, followed by a Tukey's *post hoc* test. A significance of $p < 0.05$ was required for rejection of the null hypothesis.

3. Results

3.1. Characterization of the fibermats

SEM images of the V, SiV, and MgSiV particles are shown in Figure 1, and their diameters were approximately 0.6, 1.1, and 1.1 μ m, respectively. The densities of V, SiV, and MgSiV were 2.54 ± 0.09 , 2.24 ± 0.03 , and 2.27 ± 0.07 g·cm⁻³, respectively. The number-average molecular weight (M_n), weight-average molecular weight (M_w), and polydispersity index (PDI, M_w/M_n) of the composites are listed in Table 1. The composites indicated a smaller M_n and larger PDI than those of PLLA.

The SEM images of the VPC_x , $SiVPC_x$, and $MgSiVPC_x$ fibermats are shown in Figure 2, and their fiber diameters are shown in Figure 3. The fiber diameters of the fibermats were approximately 10–15 μ m; thus, the cells can adhere on a single fiber [28]. Hereafter, the fibermats of VPC_7 , $SiVPC_8$, and $MgSiVPC_{12}$ were selected to evaluate their properties because their fiber diameters were similar and showed better yields than the other fibermats. The fiber orientation angle histograms of VPC_7 , $SiVPC_8$, and $MgSiVPC_{12}$ are shown in Figure 4, and the angles were distributed about a center of zero. The calculated FD values of VPC_7 , $SiVPC_8$, and $MgSiVPC_{12}$ were 0.92 ± 0.05 , 0.86 ± 0.09 , and 0.73 ± 0.18 , respectively.

The ion-releasing behaviors of VPC_7 , $SiVPC_8$, and $MgSiVPC_{12}$ are shown in Figure 5(a–c). A dashed line indicates 0 mM, representing the ion concentration in the α -MEM. The released amount of Ca²⁺ ions from the fibermats into the α -MEM increased with an increasing soaking time. That of the Mg²⁺ ions from $MgSiV_{12}$ also increased with an

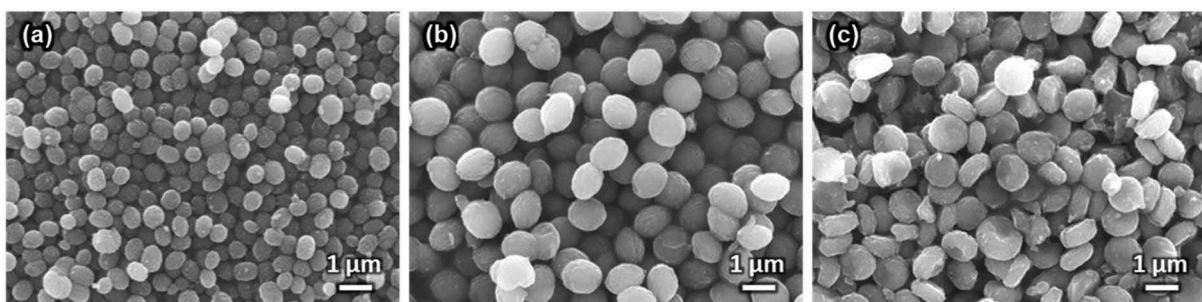


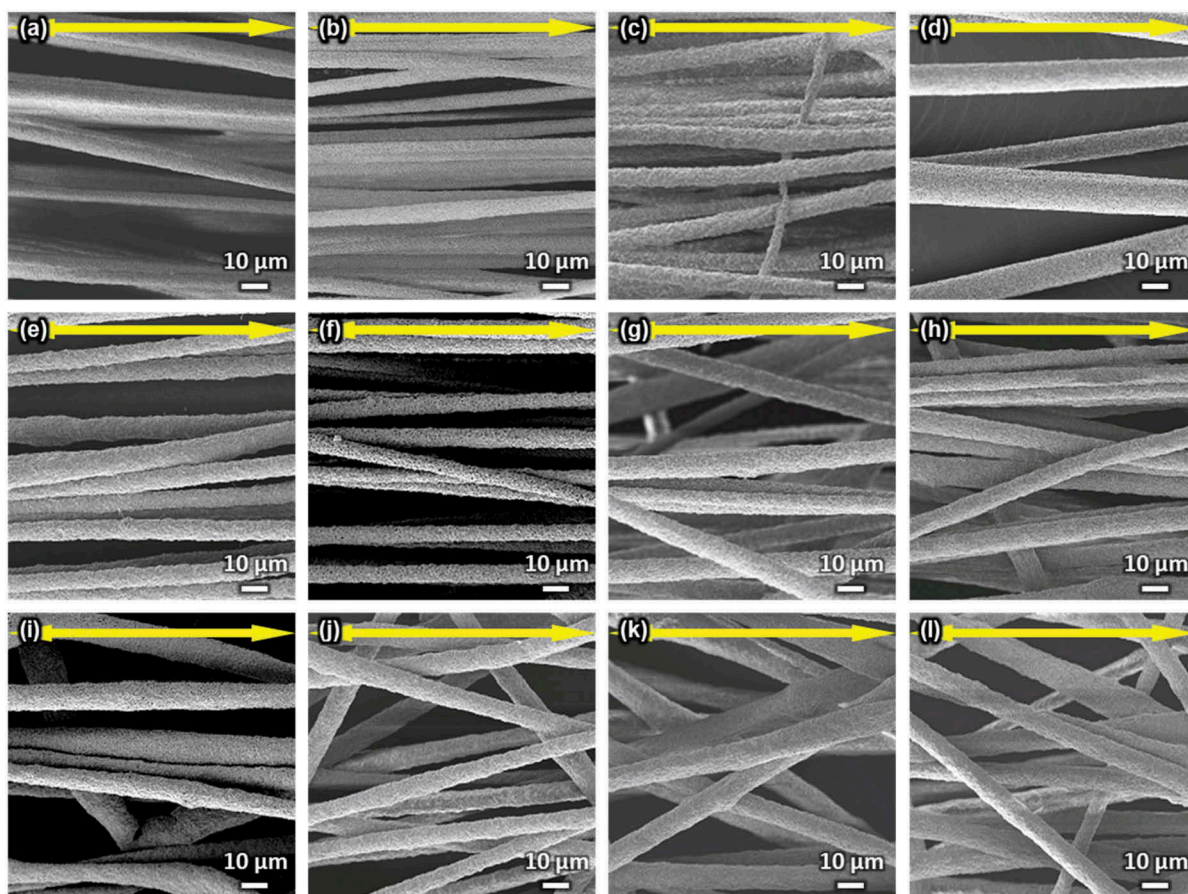
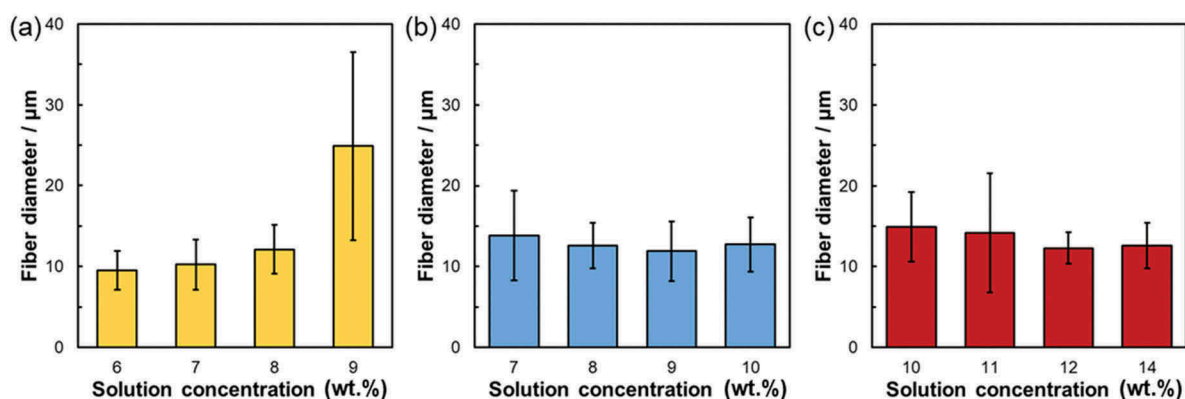
Figure 1. SEM images of (a) V, (b) SiV, and (c) MgSiV.

Table 1. Molecular weights and polydispersity indices (M_w/M_n) of PLLA, VPC, SiVPC, and MgSiVPC.

Sample code	M_n /kDa	M_w /kDa	M_w/M_n
PLLA	58.5	108.7	1.9
VPC	42.7	102.1	2.4
SiVPC	41.0	99.6	2.4
MgSiVPC	52.4	109.4	2.1

increasing soaking time. The silicate-ion-releasing behaviors from SiVPC₈ and MgSiVPC₁₂ drastically increased during day 1 of soaking, and there was no significant difference in the amount of silicate

ions released after day 1. The phosphate-ion-releasing behaviors from SiVPC₈ and MgSiVPC₁₂ decreased with an increasing soaking time. The XRD patterns of VPC₇, SiVPC₈, and MgSiVPC₁₂ after soaking in the α -MEM for 21 days are shown in Figure 5(d). VPC₇ and SiVPC₈ showed XRD peaks corresponding to vaterite (V, CaCO₃, ICDD card: 74-1867) and calcite (CaCO₃, ICDD card: 83-0578). SiVPC₈ and MgSiVPC₁₂ showed peaks corresponding to hydroxyapatite (HA, Ca₁₀(PO₄)₆(OH)₂, ICDD card: 74-0566).

**Figure 2.** SEM images of (a) VPC₆, (b) VPC₇, (c) VPC₈, (d) VPC₉, (e) SiVPC₇, (f) SiVPC₈, (g) SiVPC₉, (h) SiVPC₁₀, (i) MgSiVPC₁₀, (j) MgSiVPC₁₁, (k) MgSiVPC₁₂, and (l) MgSiVPC₁₄. The yellow arrows indicate the collector rotation direction (0°).**Figure 3.** Fiber diameter of (a) VPC_x, (b) SiVPC_x, and MgSiVPC_x. The error bars represent the standard deviation.

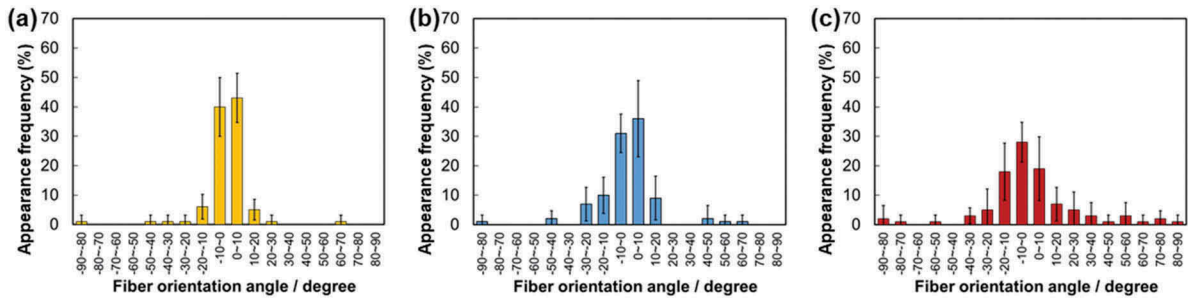


Figure 4. Fiber orientation angle histogram for (a) VPC₇, (b) SiVPC₈, and (c) MgSiVPC₁₂. The error bars represent the standard deviation.

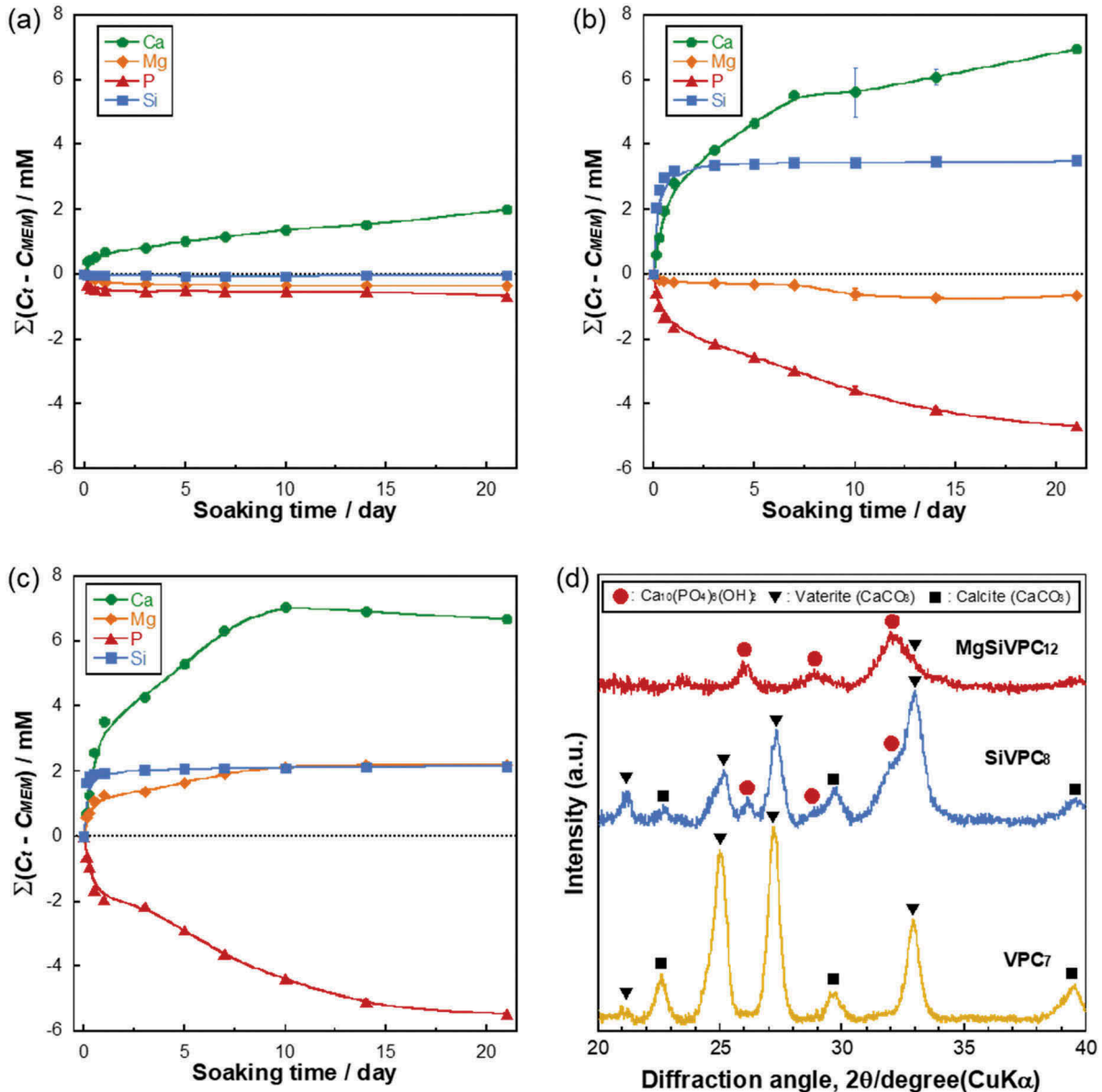


Figure 5. Accumulative ion concentration calculated with $\sum(C_t - C_{MEM})$ for (a) VPC₇, (b) SiVPC₈, and (c) MgSiVPC₁₂, where C_t is the concentration of the element in the α -MEM with VPC₇, SiVPC₈, and MgSiVPC₁₂ at time point t , and C_{MEM} is the element concentration in the α -MEM. The error bars represent the standard deviation. The dashed line indicates 0 mM, representing the ion concentration in the α -MEM. Image (d) shows the XRD patterns of the fibermats after soaking in α -MEM for 21 days.

3.2. Cell behavior on the fibermats

The fluorescence images of the cells and cell orientation angle histograms are shown in Figure 6. The cells were adhered on the single fiber surfaces and were

aligned in the fiber-oriented direction (i.e. the collector rotation direction). Their orientation angles were distributed about a center of zero. The calculated cell orientation degrees (CD) on the fibermats for VPC₇,

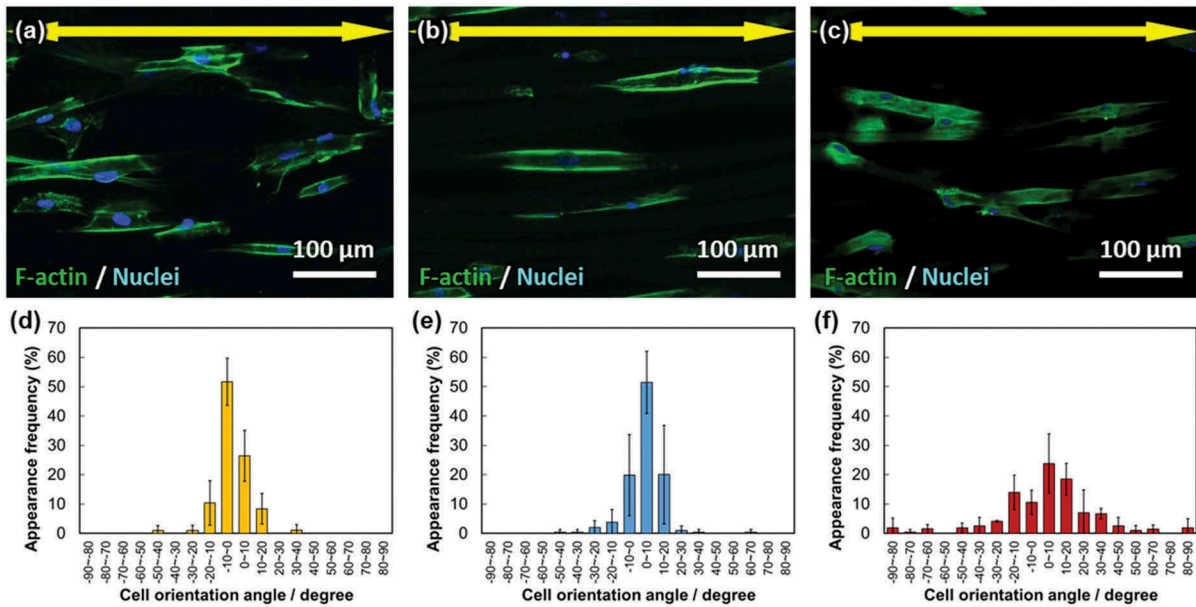


Figure 6. Fluorescence images of the primary osteoblasts cultured on (a) VPC₇, (b) SiVPC₈, and (c) MgSiVPC₁₂. The yellow arrows indicate the collector rotation direction (0°): green: F-actin and blue: nuclei. The cell orientation angle histograms are shown for (d) VPC₇, (e) SiVPC₈, and (f) MgSiVPC₁₂. The error bars represent the standard deviation.

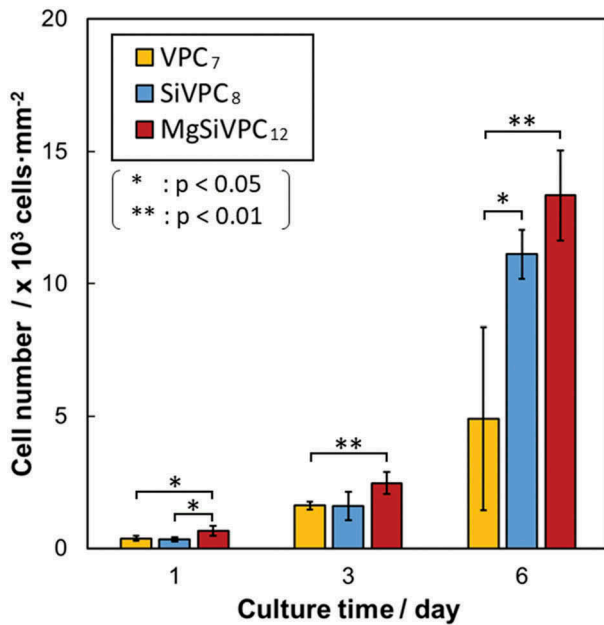


Figure 7. Cell numbers after 1–6 days on the fiber mats. The error bars represent the standard deviation.

SiVPC₈, and MgSiVPC₁₂ were 0.95 ± 0.01 , 0.93 ± 0.02 , and 0.66 ± 0.07 , respectively. In Figure 7, the number of cells on MgSiVPC₁₂ was significantly larger than that of the other fiber mats at day 1, and those of SiVPC₈ and MgSiVPC₁₂ were significantly larger than that of VPC₇ at day 6.

4. Discussion

The density of V ($2.54 \text{ g}\cdot\text{cm}^{-3}$) was smaller than that of the reference (ICCD card: 74–1867) at $2.66 \text{ g}\cdot\text{cm}^{-3}$

because V contains a small amount of amorphous calcium carbonate [30]. SiV and MgSiV had smaller densities than that of V owing to the silsesquioxane and amorphous calcium carbonate phases [15,30]. Obata *et al.* reported that the scission of the PLLA chain was induced by the shear stress generated during the melt-blending process [14,35]. Thus, M_n and M_w of VPC, SiVPC, and MgSiVPC were less than those of PLLA.

In electrospinning, polymer fibers are formed by the creation and elongation of an electric field fluid jet [36]. The velocities of the jets measured using a high frame-rate video camera were in the range of 0.5 to $5.0 \text{ m}\cdot\text{s}^{-1}$ [36]. In this work, a collector speed of $4.7 \text{ m}\cdot\text{s}^{-1}$ was used to prepare the fiber mats. The fibers could be collected while elongating in the collector rotation direction. During the electrospinning process, the solution formed a single stable jet in this work. Accordingly, the fiber diameter can be estimated as follows:

$$R = K_s \times 2 \sqrt{\frac{F}{\pi v_c}} \quad (4)$$

where R is the diameter of the fiber (m); K_s is the shrinkage ratio of the fiber; F is the flow rate of the electrospinning solution ($\text{L}\cdot\text{s}^{-1}$), and v_c is the collecting speed ($\text{m}\cdot\text{s}^{-1}$). The parameter R was calculated to be $26 \mu\text{m}$, when K_s was 1.0 (i.e. the fiber did not shrink). However, the fibers will shrink during the electrospinning process owing to the evaporation of the chloroform. The parameter K_s can be estimated as follows with the assumption that the fibers were densely packed without pores:

$$K_s = \left(\frac{x}{\rho_{PLLA}} + \frac{\{y/(100-y)\} \times x}{\rho_{powder}} \right) / \left(\frac{x}{\rho_{PLLA}} + \frac{\{y/(100-y)\} \times x}{\rho_{powder}} + \frac{100-x}{\rho_{CHCl_3}} \right) \quad (5)$$

where x is the wt.% of PLLA in the electrospinning solution; y is the wt.% of powder in the composites; ρ_{PLLA} is the density of PLLA ($1.25 \text{ g}\cdot\text{cm}^{-3}$); ρ_{powder} is the density of the V, SiV, and MgSiV powders, and ρ_{CHCl_3} is the density of chloroform ($1.49 \text{ g}\cdot\text{cm}^{-3}$). The calculated fiber diameters of VPC₇, SiVPC₈, and MgSiVPC₁₂ were 3.5, 4.2, and 6.0 μm , respectively, with K_s obtained from Equation (5). However, the measured fiber diameters of VPC₇, SiVPC₈, and MgSiVPC₁₂ were 10.2 ± 3.1 , 12.6 ± 2.8 , and $12.3 \pm 1.9 \mu\text{m}$, respectively. During the electrospinning process, pores were formed through the evaporation of the chloroform [35,37]. Figure 8 shows a highly magnified view of the VPC₇, SiVPC₈, and MgSiVPC₁₂ fiber surfaces. The evaporation pores were confirmed on their surfaces in the elongated longitudinal direction. Thus, the evaporation pores could cause the fiber-diameter difference between the calculated and measured results. According to Sun *et al.*, the cells can adhere on a single fiber for a fiber diameter $> 10 \mu\text{m}$ [28]. The diameters of VPC₇, SiVPC₈, and MgSiVPC₁₂ were larger than $10 \mu\text{m}$; therefore, the cell orientation could be controlled with the fiber orientation of the fiber mats.

In our previous study, the collagen matrix produced aligned primary osteoblasts oriented in the direction of cellular elongation, and the c -axis of the deposited apatite crystals showed preferential alignment along the direction of the collagen matrix [7]. Thus, strongly oriented osteoblasts can produce anisotropic bone tissue. In Figure 6, the primary osteoblasts were attached on the single fiber; therefore, the cell alignment can be controlled by the fiber orientation. Figure 9 shows the correlation between FD and CD . The average FD of the fiber mats is the x -axis, and the CD for each fiber mat ($n = 3$) is the y -axis. FD and CD showed a strong positive correlation ($p < 0.01$, $R^2 = 0.88$); thus, the cell alignment was controlled by the morphology of the fiber mats. These results indicated that the cell orientation could be freely

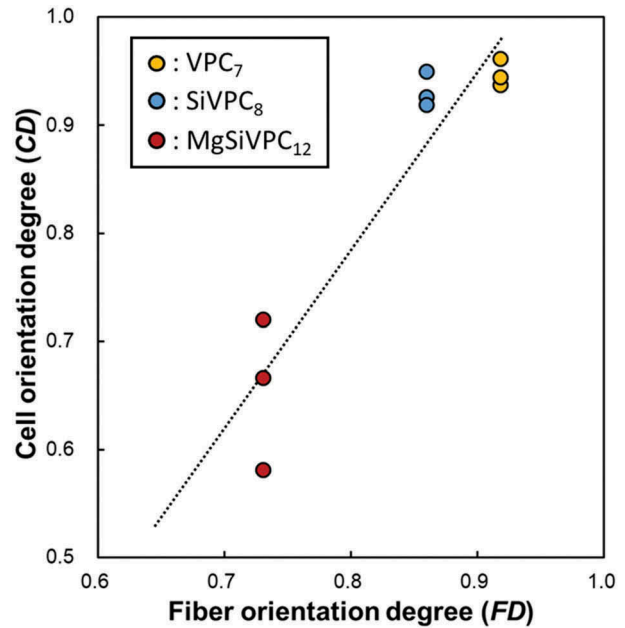


Figure 9. Correlation between the fiber orientation degree (FD) and cell orientation degree (CD). The average FD of the fiber mats is the x -axis, and the CD for each fiber mat ($n = 3$) is the y -axis. The dashed line represents the correlation between FD and CD .

manipulated by controlling the fiber orientation. Accordingly, the directional control of osteoblasts using the morphology of the scaffolds could affect the formation of anisotropic bone tissue (i.e. bone quality).

The amount of silicate ions released from SiVPC₈ and MgSiVPC₁₂ increased within 24 h, showing similar trends with that of the particles [15,30,31] because of the fast Si-O-Si hydrolysis of the amino-propyl-functionalized siloxane and the dissolution of the uncondensed APTES molecules [30,38]. The phosphate-ion-releasing behaviors of SiVPC₈ and MgSiVPC₁₂ decreased with an increasing soaking time owing to the precipitation of HA. VPC₇ and SiVPC₈ showed calcite peaks owing to the dissolution of V and the induction of calcite recrystallization [39]. The number of cells for MgSiVPC₁₂ was significantly larger than that for VPC₇ after 1 and 3 days of culture. This was caused by the dissolved Mg^{2+} ion from MgSiVPC₁₂, which

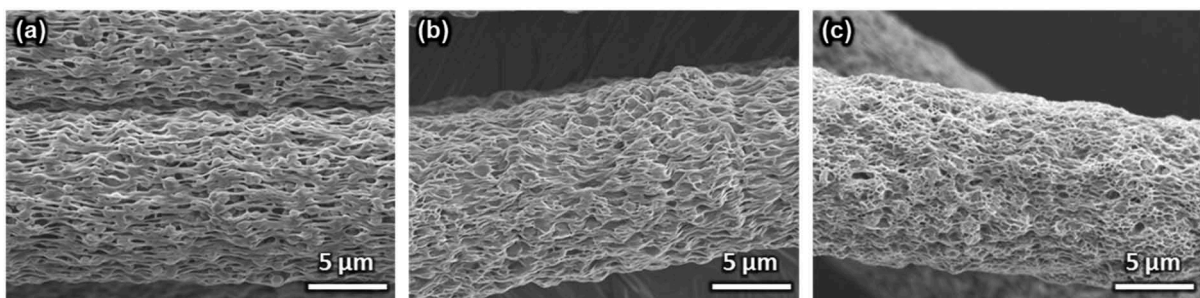


Figure 8. SEM images of (a) VPC₇, (b) SiVPC₈, and (c) MgSiVPC₁₂ with a highly magnified view.

improved cell adhesion and proliferation [17,22–24]. At day 6, the number of cells for SiVPC₈ and MgSiVPC₁₂ was larger than that of VPC₇ because the dissolved silicate ions enhanced cell proliferation [18]. Obata *et al.* reported that the MC3T3-E1 cells on the SiV/PLLA composite film showed larger cell numbers and ALP activity than those on the V/PLLA composite film [13]. In addition, an *in vivo* test showed that newly formed bone was induced inside of the random SiV/PLLA fibermats [14]. Yamada *et al.* reported that the released ions from the MgSiV particles enhanced the cell adhesion, proliferation, differentiation, and following calcification [17]. Accordingly, SiVPC₈ and MgSiVPC₁₂ can effectively enhance bone formation (i.e. bone quantity) because of the released silicate and/or Mg²⁺ ions from the fibermats.

5. Conclusion

A novel scaffold for bone regeneration that could control the osteoblast alignment and proliferation was established. The fiber diameter and orientation were designed to create strong cell alignment by controlling the electrospinning conditions. The oriented SiVPC and MgSiVPC composite fibermats enabled cell alignment along the fibers and stimulated cell adhesion and proliferation owing to the released ions from SiV and MgSiV. The cells were adhered along the single fibers, and their alignment was controlled by the morphology of the fibermats. The obtained results indicated that the fabricated composites could control the arrangement of the osteoblasts by the morphology of the fibermats, and the released ions improved the osteoblast adhesion and proliferation. Innovative scaffolds for tissue regeneration were developed using optimization of the morphology of the scaffolds and inorganic ion release.

Acknowledgments

The authors thank Dr Yoshio Ota (Yabashi Industries Co.) for supporting this work.

Disclosure statement

No potential conflict of interest was reported by the authors.

Funding

This work was supported in part by Japan Society for the Promotion of Science KAKENHI grant numbers JP18H05254, JP17H06224, and JP16K14403.

ORCID

Sungho Lee  <http://orcid.org/0000-0002-4367-9573>

References

- [1] Weiner S, Wagner HD. The material bone: structure-mechanical function relations. *Annu Rev Mater Sci.* 1998;28:271–298.
- [2] Nakano T. Bone tissue and biomaterial design based on the anisotropic microstructure. In: Niinomi M, Narushima T, Nakai M, editors. *Advances in metallic biomaterials: tissues, materials and biological reactions.* Berlin, Heidelberg: Springer Berlin Heidelberg; 2015. p. 3–30.
- [3] Seto J, Gupta HS, Zaslansky P, et al. Tough lessons from bone: extreme mechanical anisotropy at the mesoscale. *Adv Funct Mater.* 2008;18:1905–1911.
- [4] Nakano T, Kaibara K, Tabata Y, et al. Unique alignment and texture of biological apatite crystallites in typical calcified tissues analyzed by microbeam x-ray diffractometer system. *Bone.* 2002;31:479–487.
- [5] Ishimoto T, Nakano T, Umakoshi Y, et al. Degree of biological apatite c-axis orientation rather than bone mineral density controls mechanical function in bone regenerated using recombinant bone morphogenetic protein-2. *J Bone Miner Res.* 2013;28:1170–1179.
- [6] Nakano T, Kaibara K, Ishimoto T, et al. Biological apatite (BAP) crystallographic orientation and texture as a new index for assessing the microstructure and function of bone regenerated by tissue engineering. *Bone.* 2012;51:741–747.
- [7] Matsugaki A, Isobe Y, Saku T, et al. Quantitative regulation of bone-mimetic, oriented collagen/apatite matrix structure depends on the degree of osteoblast alignment on oriented collagen substrates. *J Biomed Mater Res A.* 2015;103:489–499.
- [8] Ozasa R, Matsugaki A, Isobe Y, et al. Construction of human induced pluripotent stem cell-derived oriented bone matrix microstructure by using *in vitro* engineered anisotropic culture model. *J Biomed Mater Res A.* 2018;106:360–369.
- [9] Madhurakkat Perikamana SK, Lee J, Ahmad T, et al. Effects of immobilized BMP-2 and nanofiber morphology on *in vitro* osteogenic differentiation of hMSCs and *in vivo* collagen assembly of regenerated bone. *ACS Appl Mater Interfaces.* 2015;7:8798–8808.
- [10] Lee J-H, Lee YJ, Cho H-J, et al. Guidance of *in vitro* migration of human mesenchymal stem cells and *in vivo* guided bone regeneration using aligned electrospun fibers. *Tissue Eng Part A.* 2013;20:2031–2042.
- [11] Chen X, Fu X, Shi J-G, et al. Regulation of the osteogenesis of pre-osteoblasts by spatial arrangement of electrospun nanofibers in two- and three-dimensional environments. *Nanomed Nanotechnol Biol Med.* 2013;9:1283–1292.
- [12] Matsugaki A, Aramoto G, Ninomiya T, et al. Abnormal arrangement of a collagen/apatite extracellular matrix orthogonal to osteoblast alignment is constructed by a nanoscale periodic surface structure. *Biomaterials.* 2015;37:134–143.
- [13] Obata A, Tokuda S, Kasuga T. Enhanced *in vitro* cell activity on silicon-doped vaterite/poly(lactic acid) composites. *Acta Biomater.* 2009;5:57–62.
- [14] Obata A, Hotta T, Wakita T, et al. Electrospun microfiber meshes of silicon-doped vaterite/poly(lactic

- acid) hybrid for guided bone regeneration. *Acta Biomater.* **2010**;6:1248–1257.
- [15] Yamada S, Ota Y, Nakamura J, et al. Preparation of siloxane-containing vaterite doped with magnesium. *J Ceram Soc Jpn.* **2014**;122:1010–1015.
- [16] Yamada S, Obata A, Maeda H, et al. Development of magnesium and siloxane-containing vaterite and its composite materials for bone regeneration. *Front Bioeng Biotechnol.* **2015**;3:195.
- [17] Yamada S, Ota Y, Obata A, et al. Osteoblast-like cell responses to ion products released from magnesium- and silicate-containing calcium carbonates. *Biomed Mater Eng.* **2017**;28:47–56.
- [18] Xynos ID, Edgar AJ, Buttery LDK, et al. Ionic products of bioactive glass dissolution increase proliferation of human osteoblasts and induce insulin-like growth factor II mRNA expression and protein synthesis. *Biochem Biophys Res Commun.* **2000**;276:461–465.
- [19] Xynos ID, Hukkanen JMV, Batten JJ, et al. Bioglass®45S5 stimulates osteoblast turnover and enhances bone formation in vitro: implications and applications for bone tissue engineering. *Calcif. Tissue Int.* **2000**;67:321–329.
- [20] Maeno S, Niki Y, Matsumoto H, et al. The effect of calcium ion concentration on osteoblast viability, proliferation and differentiation in monolayer and 3D culture. *Biomaterials.* **2005**;26:4847–4855.
- [21] Marie PJ. The calcium-sensing receptor in bone cells: A potential therapeutic target in osteoporosis. *Bone.* **2010**;46:571–576.
- [22] Zreiqat H, Howlett CR, Zannettino A, et al. Mechanisms of magnesium-stimulated adhesion of osteoblastic cells to commonly used orthopaedic implants. *J Biomed Mater Res.* **2002**;62:175–184.
- [23] Takeichi M, Okada TS. Roles of magnesium and calcium ions in cell-to-substrate adhesion. *Exp Cell Res.* **1972**;74:51–60.
- [24] Wolf FI, Cittadini A. Magnesium in cell proliferation and differentiation. *Front Biosci.* **1999**;4:D607–D617.
- [25] Kasuga T, Obata A, Maeda H, et al. Siloxane-poly(lactic acid)-vaterite composites with 3D cotton-like structure. *J Mater Sci Mater Med.* **2012**;23:2349–2357.
- [26] Wang J, Zhou P, Obata A, et al. Preparation of cotton-wool-like poly(lactic acid)-based composites consisting of core-shell-type fibers. *Materials.* **2015**;8:7979–7987.
- [27] Lee S, Matsugaki A, Kasuga T, et al. Development of bifunctional oriented bioactive glass/poly(lactic acid) composite scaffolds to control osteoblast alignment and proliferation. *J Biomed Mater Res A.* **2019**;107:1031–1041.
- [28] Sun T, Norton D, McKean RJ, et al. Development of a 3D cell culture system for investigating cell interactions with electrospun fibers. *Biotechnol Bioeng.* **2007**;97:1318–1328.
- [29] Kasuga T, Maeda H, Kato K, et al. Preparation of poly(lactic acid) composites containing calcium carbonate (vaterite). *Biomaterials.* **2003**;24:3247–3253.
- [30] Nakamura J, Poologasundarampillai G, Jones JR, et al. Tracking the formation of vaterite particles containing aminopropyl-functionalized silsesquioxane and their structure for bone regenerative medicine. *J Mater Chem B.* **2013**;1:4446–4454.
- [31] Nakamura J, Kasuga T. Enhancement of crystalline plane orientation in silsesquioxane-containing vaterite particles towards tuning of calcium ion release. *J Mater Chem B.* **2014**;2:1250–1254.
- [32] Matsugaki A, Fujiwara N, Nakano T. Continuous cyclic stretch induces osteoblast alignment and formation of anisotropic collagen fiber matrix. *Acta Biomater.* **2013**;9:7227–7235.
- [33] Wong G, Cohn DV. Separation of parathyroid hormone and calcitonin-sensitive cells from non-responsive bone cells. *Nature.* **1974**;252:713.
- [34] Umeno A, Kotani H, Iwasaka M, et al. Quantification of adherent cell orientation and morphology under strong magnetic fields. *IEEE Trans Magn.* **2001**;37:2909–2911.
- [35] Obata A, Ozasa H, Kasuga T, et al. Cotton wool-like poly(lactic acid)/vaterite composite scaffolds releasing soluble silica for bone tissue engineering. *J Mater Sci Mater Med.* **2013**;24:1649–1658.
- [36] Reneker DH, Yarin AL. Electrospinning jets and polymer nanofibers. *Polymer.* **2008**;49:2387–2425.
- [37] Sill TJ, von Recum HA. Electrospinning: applications in drug delivery and tissue engineering. *Biomaterials.* **2008**;29:1989–2006.
- [38] Nakamura J, Kasuga T. Preparation of siloxane-containing vaterite particles with red-blood-cell-like morphologies and incorporation of calcium-salt polylactide for bone regenerative medicine. *J Ceram Soc Jpn.* **2013**;121:792–796.
- [39] Nakamura J, Ota Y, Sakka Y, et al. Interphase coordination design in carbamate-siloxane/vaterite composite microparticles towards tuning ion-releasing properties. *Adv Powder Technol.* **2017**;28:1349–1355.